Philosophical Magazine

ISSN: 0031-8086 (Print) (Online) Journal homepage: http://www.tandfonline.com/loi/tphm19

The role of charge density waves in structural transformations of 1T TaS_2

C. B. Scruby , P. M. Williams & G. S. Parry

To cite this article: C. B. Scruby , P. M. Williams & G. S. Parry (1975) The role of charge density waves in structural transformations of 1T TaS_2 , Philosophical Magazine, 31:2, 255-274, DOI: 10.1080/14786437508228930

To link to this article: https://doi.org/10.1080/14786437508228930

Published online: 02 Sep 2006.

The role of charge density waves in structural transformations of 1T TaS_2

By C. B. Scruby, P. M. Williams and G. S. Parry

Department of Chemical Engineering and Chemical Technology, Imperial College, London SW7 2BY, England

[Received 4 October 1974 and after revision 17 October 1974]

Abstract

Electron and X-ray diffraction studies have identified three metastable phases in 1T TaS_2. Extra reflexions are interpreted as arising from charge density waves coupled to periodic distortions modulating a trigonal lattice. These waves are incommensurate with the matrix in $1T_1$ and $1T_2$, but form a commensurate superlattice in $1T_3$. Within $1T_2$, the temperature dependence of the wave vector is correlated with a change in the cross-section of the Fermi surface, while the diffuse scattering which accompanies the discrete reflexions in $1T_1$ is discussed as an image of this surface in the phonon spectrum. Changes in the stacking of distortions and in their amplitude are also reported.

§ 1. Introduction

It has been suggested (Williams, Parry and Scruby 1974) that the diffuse streaking present in electron and X-ray diffraction studies of 1T TaS_2 above 350 K (phase $1T_1$) arises because of a Kohn screening anomaly in the tantalum 5*d* conduction electrons. The logarithmic singularity in the dielectric constant for a phonon of wave vector $\mathbf{q}$ which just spans the Fermi surface (Kohn 1959) is an example of the instability displayed by a system of conduction electrons with respect to a spatially varying perturbation for which $\mathbf{q} = 2\mathbf{k}_F$ (Chan and Heine 1973). If this instability takes the form of a spin density wave (Overhauser 1962) then the perturbation is detectable by neutron diffraction (Bacon 1962).

The alternative, a charge density wave (Overhauser 1968), is stable only if coupled to a periodic lattice distortion (Chan and Heine 1973), and such distortions will be detectable by electron and X-ray diffraction if the distortion amplitude is a significant fraction of the matrix lattice periodicity. If this condition is satisfied, the periodic lattice distortion can be directly imaged in the electron microscope (Scruby, in preparation). Distortions of this magnitude arise because those phonon modes which are associated with the Kohn anomaly are softened progressively as the anomaly becomes stronger, i.e. as areas of the Fermi surface become progressively more flat and parallel (Afanasev and Kagan 1963, Fehlner and Loly 1974). If the phonon mode is softened completely, the deformations become static and it might be expected that these distortions would be arranged in a regular way. This has already been proposed as the reason why sharp extra reflexions accompany the diffuse streaking in diffraction photographs in $1T_1$ and the idea is explored in greater depth in the present paper.

When these two diffraction effects are observed, the 1T polymorph of TaS_2 is thermodynamically unstable and changes irreversibly to the stable 2H phase at a somewhat higher temperature. Both polymorphs are sandwich layer structures in which the metal atoms are coordinated by two planes of sulphur atoms so that the tantalum site symmetry is octahedral in the undistorted 1T polymorph and trigonal prismatic in the 2H polymorph (Jellinek 1962, Wilson and Yoffe 1969). The transformation 1T→2H therefore involves the passage of an intralayer dislocation which changes the stacking sequence from *AbC* to *AbA* (or *CbC*). As this is a major solid-state transformation, it is not surprising that the 1T polymorph, which is the stable form at crystal growth temperatures (~ 1250 K), can readily be quenched to a temperature at which the rate of transformation to the stable phase is negligible (< 450 K).

Quenched 1T TaS_2 exists in three forms which have been designated $1T_1$, $1T_2$ and $1T_3$ by Williams *et al.* (1974). Thus measurements of physical properties (Thompson, Gamble and Revelli 1971) show discontinuities in electrical resistance at about 350 K ($1T_1 \rightarrow 1T_2$), and centred at 190 K ($1T_2 \rightarrow 1T_3$) (fig. 1). Associated differential thermal analysis and differential scanning calorimetry measurements by these authors indicated that each transition is endothermic on heating, and it was concluded that both transformations appeared to be thermodynamically of first order even though there was no detectable volume change on going from $1T_2$ to $1T_1$. The only lattice parameter discontinuity

Fig. 1

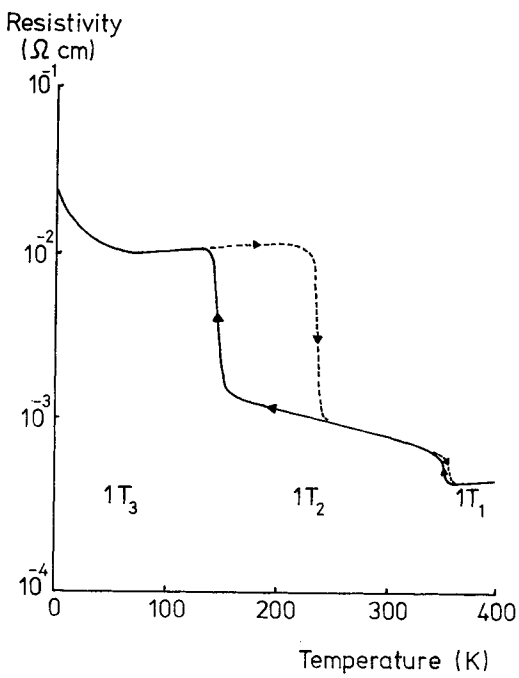

Temperature dependence of resistivity for 1T TaS_2 (Thompson, Gamble, and Revelli 1971), showing the two transitions of interest: $1T_1 \rightarrow 1T_2$, $1T_2 \rightarrow 1T_3$.

was a decrease of 0·02 Å in the hexagonal c-axis on heating through the transition $1T_3 \rightarrow 1T_2$. As is clear from fig. 1, there is a hysteresis loop of width 100 K associated with this transition.

The results of the investigation described below reveal the unusual structural behaviour of TaS_2 and emphasize that attempts to interpret its properties in conventional terms may be inappropriate. Indeed, it appears that the intermediate phase, $1T_2$, may be unique to this material. Certainly it is absent from 1T $TaSe_2$ (Wilson, DiSalvo and Mahajan 1974 a) and the mixed polytype $4H_b$ TaS_2 (Shepherd, Williams, Young and Scruby 1974) even though octahedrally coordinated layers in both these materials exhibit phases which resemble $1T_1$ and $1T_3$ tantalum disulphide.

§ 2. Experimental procedures and results

Each of the three phases was studied both by electron and by X-ray diffraction. As will be seen, the two techniques were largely complementary, and enabled a detailed picture to be obtained of the changes occurring in reciprocal space as the temperature of the metastable 1T TaS_2 phases was varied from 420 to 80 K.

For transmission electron diffraction studies (at 100 kV using JEM 7A and JEM 100B instruments) crystals of 1T TaS_2 were successively cleaved until very thin areas of specimen were obtained that were transparent to electrons. Diffraction patterns were obtained with the incident beam along the c^*-axis, i.e. perpendicular to the TaS_2 layer. It was also possible to tilt the incident beam relative to the specimen by several degrees in both instruments. Either a heating stage, or a liquid nitrogen cold stage, could be fitted to the JEM 7A microscope to enable the specimens to be studied under a wide range of temperature conditions.

For X-ray studies, small hexagonal single-crystal plates, (thickness $\sim$ 0·2 mm, hexagonal edge dimension $\sim$ 4 mm) were selected from material originating from the same source as that for electron diffraction work. These crystals were mounted on a glass fibre, using Araldite for experiments at and above room temperature and shellac for low-temperature experiments. The crystal was set and oscillated about a matrix a-axis using a Unicam S25 single-crystal goniometer, and diffraction patterns were recorded with Mo Kα radiation using a flat plate film holder. The Zr β-filter was placed immediately in front of the film rather than in the beam collimator as this improved the quality of films obtained after the long exposures which were necessary because of the high absorption by the crystal ($\mu \sim 250$ cm^{-1}). For low-temperature studies, liquid nitrogen was dripped slowly on to the crystal, while temperatures up to 420 K were obtained using a small electrically heated furnace to surround the crystal.

X-ray diffraction photographs were used to confirm the reciprocal space geometry found in transmission electron diffraction patterns with the beam parallel to $\mathbf{c}^*$. Each electron diffraction plate in this orientation (fig. 2) revealed extra reflexions surrounding every reflexion of the trigonal matrix predicted by the ideal CdI_2 structure (stacking sequence *AbC AbC*). The presence of these extra reflexions in the X-ray photographs (fig.3) showed that the direct space periodicities which they imply are characteristic of the whole

Fig. 2

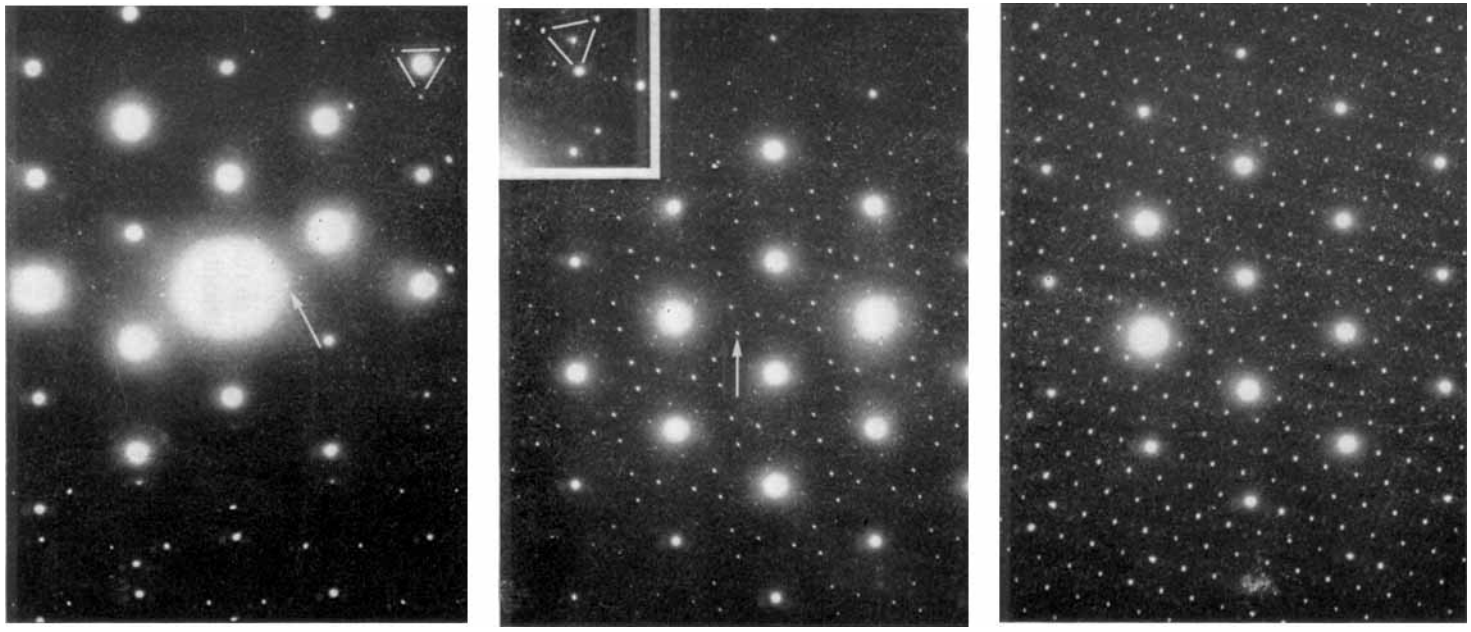

(i) $1T_1$ (ii) $1T_2$ (iii) $1T_3$

Selected area diffraction patterns with incident electron beam parallel to **c***; (i) $1T_1$ at 340 K, identifying the triangular grouping $\{\mathbf{S}_M(10{\cdot}1)\}$ and indicating by arrow one $\mathbf{S}_M(11{\cdot}0)$ reflexion near the origin; (ii) $1T_2$ at 290 K, the arrow indicating a $\mathbf{S}_M(11{\cdot}0)$ reflexion, and the inset showing a triangular grouping $\{\mathbf{S}_M(10{\cdot}1)\}$ when the incident beam is tilted slightly; (iii) $1T_3$ TaS_2 at 150 K.

Fig. 3

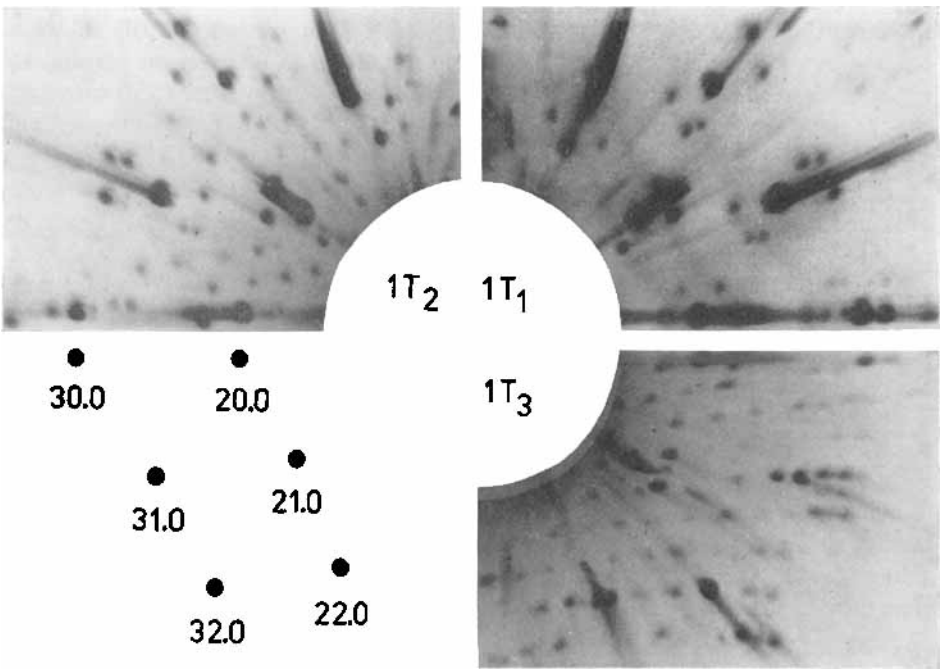

Oscillation X-ray photographs with incident beam in similar orientation to fig 2. for (i) $1T_1$ at 390 K, (ii) $1T_2$ at 290 K, (iii) $1T_3$ at 80 K, confirming the reciprocal geometry given by electron diffraction. Distortion amplitude too small in $1T_1$ for $\{\mathbf{S}_M(11{\cdot}0)\}$ to be observed.

crystal. Within experimental error, these matrix reflexions in the electron diffraction patterns do not deviate from trigonal symmetry, in agreement with the findings of Jellinek (1962).

Tilting the electron beam by several degrees showed a marked change in the diffraction pattern of $1T_2$ (fig. 2(ii) inset) and further additional reflexions appear around each matrix reflexion. The slight curvature of the $1T_1$ crystal enabled these additional reflexions to be visible near the edge of the plate (fig. 2(i)) without needing to tilt the incident beam. Tilting the electron beam produced no significant alteration in the pattern for $1T_3$ TaS_2. Figure 4 (showing reciprocal cells for each phase) enables the extra reflexions to be indexed. The position of these new reflexions relative to the *hk*.0 plane of the matrix reciprocal lattice was precisely determined using X-ray diffraction photographs taken perpendicular to **c*** (fig. 5). In the case of $1T_3$, the transformation from $1T_2$ introduced some irreversible damage, limiting the amount of information recoverable from the X-ray photograph.

Detailed consideration of the results is deferred to the next section, but briefly the triangular groupings visible in figs. 2(i) and (ii) are disposed about each matrix reflexion at heights $(l \pm \frac{1}{3})\mathbf{c}^*$ (figs. 5 (i) and (ii)), and conform to the centrosymmetric point group $\bar{3}m$ about the matrix reflexion. In $1T_1$ all the symmetry elements of the octahedron are parallel to those of the matrix reciprocal lattice, but in $1T_2$ only the $\bar{3}$ axis remains parallel as a result of a

change of about 12° in the orientation of the octahedron about this axis. In $1T_3$ the octahedron disappears and the diffraction pattern (fig. 2 (iii)) indicates a conventional hexagonal superlattice of side $\sqrt{13}\ a$. Figure 5 (iii) shows a change in the positions of the superlattice reflexions in a direction parallel to **c***, compared with $1T_1$ and $1T_2$. What these new positions mean in terms of the translational repeat distance of the $\sqrt{13}\ a \times \sqrt{13}\ a$ cell in the *c*-axis direction will be discussed later.

Some qualitative diffraction intensity data on the extra reflexions were obtained from the X-ray photographs of $1T_1$ and $1T_2$, but no quantitative study of the low-temperature $1T_3$ phase was attempted. Although it was not possible to measure the transition temperatures accurately, the $1T_2$ phase was consistently found to be stable over a slightly narrower range of temperature than that reported by Thompson *et al.* (1971). The results for all three metastable phases were reproducible in crystals of several different growth batches. This is a remarkable finding when it is realized that, as the matrix apparently remains trigonal, the present observations cannot be interpreted simply in terms of a shear transformation of the ideal CdI_2 structure. The extra reflexions from phase $1T_1$ and $1T_2$ must imply periodic distortions of the matrix lattice, and in the next section deductions from the diffraction data are considered in detail. Both in this next section and in § 4 it must be borne in mind that only the deformation of the matrix structure is under consideration.

Fig. 4

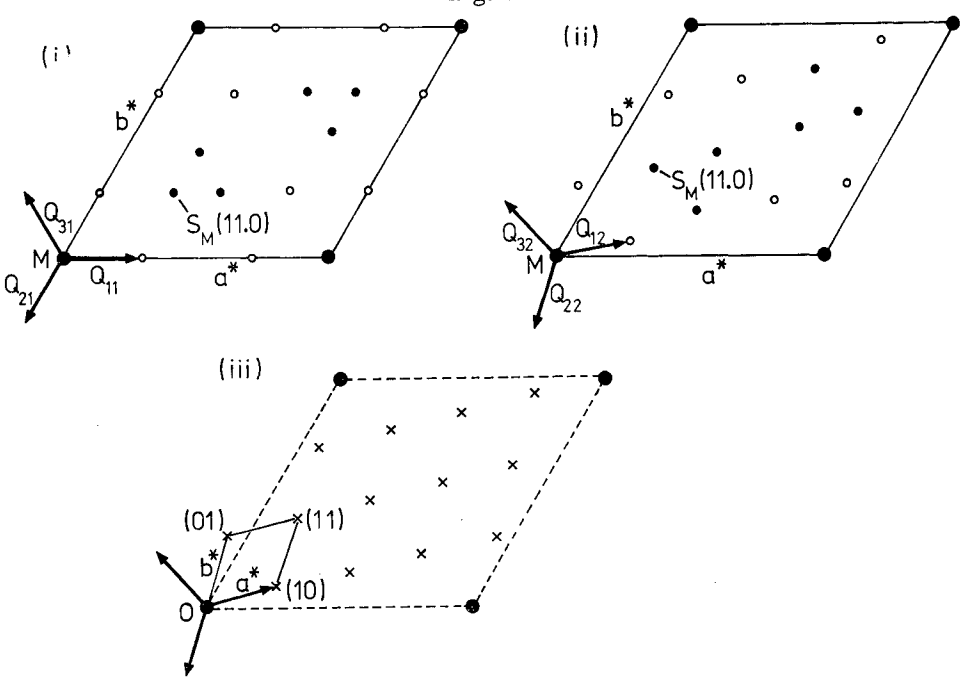

Reciprocal cells for each distorted 1T TaS_2 phase, where $\mathbf{Q}_{i1}, \mathbf{Q}_{i2}, \mathbf{Q}_{i3}$ are distortion wave vectors. In (i) $1T_1$ and (ii) $1T_2$ the unit cell is that of the matrix with: ●—$\{\mathbf{S}_M\}$ reflexions in $hk.0$ plane of **M**; ○—$\{\mathbf{S}_M\}$ reflexions at $\pm\frac{1}{3}\mathbf{c}^*$, ($\mathbf{S}_M(10{\cdot}1)$ and $\mathbf{S}_M(01{\cdot}\bar{1})$ lie at $+\frac{1}{3}\mathbf{c}^*$ and $-\frac{1}{3}\mathbf{c}^*$, respectively). In (iii) $1T_3$ the commensurate distortions define a reduced reciprocal cell, shown in projection (see text).

Fig. 5

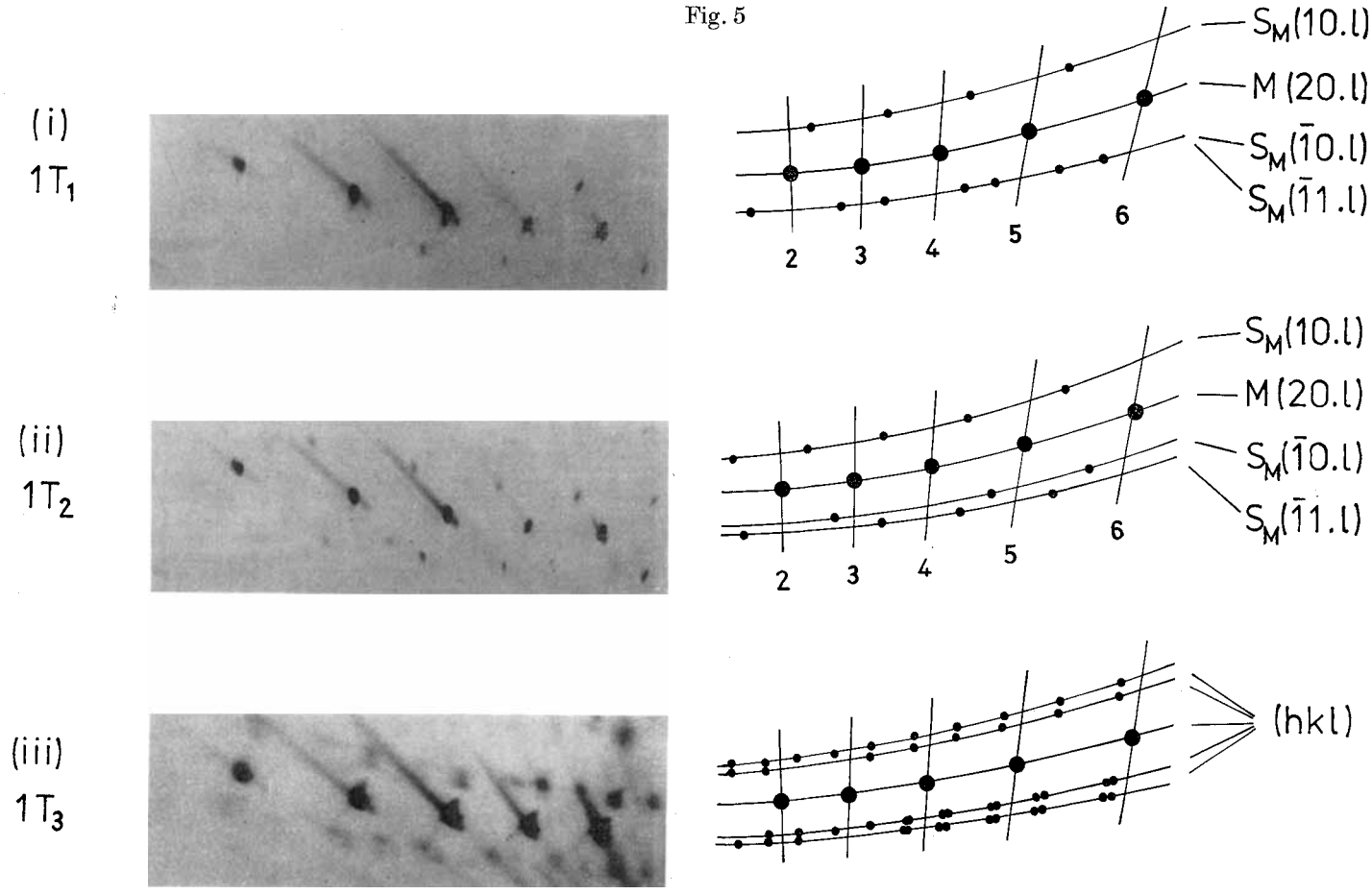

Comparison of X-ray oscillation photographs (incident beam approximately perpendicular to **c***) showing part of matrix 20 . l row, with patterns predicted by rhombohedral distortion cells in $1T_1$ and $1T_2$, and by twinned triclinic cell in $1T_3$ TaS_2 (see text). The patterns for $1T_1$ and $1T_2$ differ as a result of the change in orientation of **Q**.

§3. Interpretation of the diffraction data

3.1. *Diffraction by a distorted structure*

Since the extra reflexions are trigonally disposed about each matrix reflexion, three symmetry-related distortion waves must be considered together. Each has a wave vector $\mathbf{Q}_i=(1/2\pi)\,\mathbf{q}_i$, and amplitude $\mathbf{U}_{Q_i}$, where $|\mathbf{Q}_i|=Q_i=1/\Lambda$($\Lambda$ is the periodicity of the distortion wave in direct space) and $|\mathbf{U}_{Qi}|=U_Q=Uq$ for $i=1$, 2, 3. The layer structure of this material suggests that the distortion waves lie within each layer so that $\mathbf{Q}_i\,.\,\mathbf{c}^*=0$; experimental confirmation of this assumption will be given later (§ 3.4).

This restriction on the orientation of $\mathbf{Q}$ implies that the Fourier transform of the distortion-wave system within a single TaS_2 layer is a family of rods in reciprocal space which are perpendicular to the layer and hence parallel to $\mathbf{c}^*$. The relative phases of the distortion waves in adjacent layers modulate these rods so as to produce a set of extra reflexions $\{\mathbf{S}_M\}$, where $\mathbf{M}=h\mathbf{a}^*+k\mathbf{b}^*+l\mathbf{c}^*$ is the scattering vector of a single matrix reflexion in the set $\{\mathbf{M}\}$, and the scattering vector of any extra reflexion, $\mathbf{K}$, is given by $\mathbf{K}=\mathbf{M}+\mathbf{S}_M$. The vector $\mathbf{S}_M$ has components parallel and perpendicular to the layer. Only the latter is always commensurate with the matrix lattice, i.e. $\mathbf{S}_M\,.\,\mathbf{c}^*=1/n$, where n is 3 for $1T_1$ and $1T_2$. The vectors $\mathbf{Q}_i$ define a local coordinate system in reciprocal space and it is convenient to use this system to distinguish the integral indices of a particular $\mathbf{S}_M$ relative to $\mathbf{M}$. These indices will be written $\mathbf{S}_M(hk\,.\,l)$, where $\mathbf{S}_M=h\mathbf{Q}_1-k\mathbf{Q}_2+nl\mathbf{c}^*$.

It is well known (James 1948) that when a distortion is applied to a one-dimensional lattice so that the displacement of each atom is a periodic function of its undisplaced distance from the origin, an infinite series of 'ghosts' or 'side-bands' surrounds each diffraction maximum M that arises from the undistorted structure. These matrix reflexions occur at $\pm hg$, where $g=1/a$ and a is the direct-space periodicity of the matrix lattice. The 'ghost' extra reflexions $\{S_M\}$ occur at $\pm(hg\pm mQ)$ for integral m. The intensity of the matrix reflexion is reduced by a factor $|J_0(2\pi hgU_Q)|^2$, while the intensity of the mth-order 'ghost' is proportional to $|J_m(2\pi(hg\pm mQ)U_Q|^2$. If m is restricted to positive values the Bessel functions are approximately

$$J_0(x)=1-\tfrac{1}{4}x^2,$$

$$J_m(x)=\frac{x^m}{m!2^m}$$

for $x\ll 1$.

The theory is readily extended to three dimensions (Overhauser 1971), and in the present case of three symmetry-related distortions the intensity of a matrix reflexion at $\mathbf{M}$ will be reduced by a factor

$$\left\{1-\sum_i(\pi\mathbf{M}\,.\,\mathbf{U}_{Q_i})^2\right\}$$

and there will be six first-order $\mathbf{S}_M(10{\cdot}1)$ reflexions with intensities proportional to:

$$\tfrac{1}{4}|2\pi(\mathbf{M}\pm\mathbf{Q}_i)\,.\,\mathbf{U}_{Q_i}|^2 \text{ at } \mathbf{M}\pm(\mathbf{Q}_i+nl\mathbf{c}^*).$$

These expressions only hold when

$$(\mathbf{M}\pm\mathbf{Q}_i)\,.\,\mathbf{U}_{Q_i}\ll 1/2\pi$$

so that for the approximation to be valid, the distortion amplitude must be much

less than $1/|\mathbf{M}|$. The approximation does not hold for $|\mathbf{M}|$ large and, depending on the magnitude of U_Q, is thus applicable only to those $\mathbf{S}_M$ which lie within a fixed distance of the origin of reciprocal space.

To the same level of approximation, there will be higher-order reflexions $\mathbf{S}_M(h0\,.\,l)$, with $-1 \leqslant l \leqslant 1$, which have intensities proportional to:

$$(1/h!)^2(\tfrac{1}{2})^{2h}|2\pi(\mathbf{M} \pm h\mathbf{Q}_i)\,.\,\mathbf{U}_{Q_i}|^{2h} \text{ at } \mathbf{M} \pm h\mathbf{Q}_i + nl\mathbf{c}^*.$$

Again, extra reflexions of the type $\mathbf{S}_M(11{\cdot}0)$ will have intensities proportional to:

$$(\tfrac{1}{2})^4|2\pi(\mathbf{M}+\mathbf{Q}_1+\mathbf{Q}_2)\,.\,\mathbf{U}_{Q_1}|^2|2\pi(\mathbf{M}+\mathbf{Q}_1+\mathbf{Q}_2)\,.\,\mathbf{U}_{Q_2}|^2 \text{ at } \mathbf{M}+\mathbf{Q}_1+\mathbf{Q}_2.$$

Although this analysis was originally based on the assumption of one atom per unit cell, it can be applied to TaS_2 by assuming for the present that the distortions in the metal and non-metal sublattices have the same amplitude and phase so that the distortion waves affect metal and non-metal atoms equally. Small deviations from this idealized deformation of the sulphur layers will have little effect in diffraction as the atomic scattering factor of sulphur is only some 20% that of tantalum.

3.2. *Determination of the distortion wave vector*

The trigonal symmetry of the structure ensures that vectors related by symmetry to a given vector in reciprocal space:

$$x\mathbf{a}^* + y\mathbf{b}^*,$$

are

$$-(x+y)\mathbf{a}^* + x\mathbf{b}^*,$$

and

$$y\mathbf{a}^* - (x+y)\mathbf{b}^*.$$

Only one of these three vectors is given below.

In the $1T_1$ phase, the wave vector $\mathbf{Q}_{i1}$ of the distortion wave producing the discrete $\mathbf{S}_M$ remained always along the reciprocal axis $\mathbf{a}^*$ (figs. 2 (i) and 4 (i)). Measurements from electron diffraction patterns showed that, within experimental error, its magnitude remained in a fixed ratio to the dimensions of the reciprocal lattice throughout the range of temperature over which $1T_1$ exists, and that

$$\mathbf{Q}_{i1} = 0{\cdot}283\ \mathbf{a}^*.$$

At 340 K, the transition from $1T_1$ to $1T_2$ produced a discontinuous change both in the magnitude and in the direction of the distortion wave vector. At room temperature (figs. 2 (ii), and 4 (ii)) measurements gave

$$\mathbf{Q}_{i2} = 0{\cdot}245\ \mathbf{a}^* + 0{\cdot}068\ \mathbf{b}^*.$$

As the $1T_2$ phase was cooled from 340 K towards the transition to $1T_3$ at 190 K, there was a continuous *decrease* in the absolute magnitude of Q_{i2} as well as in its value relative to the reciprocal lattice dimensions, and an increase in the angle between $\mathbf{Q}_{i2}$ and $\mathbf{a}^*$ from 11·6° to 14° ($\tan^{-1}(\sqrt{3}/7)$).

At 190 K, $\mathbf{Q}$ ceased to be incommensurate, and defined a $\sqrt{13}\,a \times \sqrt{13}\,a$ superlattice in the $1T_3$ phase (figs. 2 (iii) and 4 (iii)). The distortion wave

vector $\mathbf{Q}_3$ remained fixed at temperatures below the transition, with

$$\mathbf{Q}_{i3} = 3/13\ \mathbf{a}^* + 1/13\ \mathbf{b}^*,$$
$$= 0{\cdot}231\ \mathbf{a}^* + 0{\cdot}077\ \mathbf{b}^*,$$

Changes in the distortion wave vector with temperature are summarized in the table.

The variation of the distortion wave vector $\mathbf{Q}$ with temperature in 1T TaS_2; $\mathbf{a}^*$ is the matrix reciprocal lattice vector, and ϕ is the angle between $\mathbf{Q}$ and $\mathbf{a}^*$.

Phase	Temperature	Q/a^*	ϕ
$1T_1$	420–340 K	0·283	0°
$1T_2$	331 K	0·286	11·6°
	303 K	0·285	12·0°
	290 K	0·285	12·1°
	269 K	0·283	12·7°
	250 K	0·282	13·1°
$1T_3$	Below 190 K	0·277	13·9°

3.3 *Stacking of distortion waves in adjacent layers*

The modulation of the reciprocal lattice rods corresponding to the wave vector $\mathbf{Q}$ gives discrete reflexions in X-ray diffraction (fig. 5), implying a strong phase correlation between radiation scattered by distortion waves in different layers. Both in $1T_1$ and in $1T_2$ the relative positions of the distortions are such that there is reinforcement of scattered radiation along the rods at $(l+\frac{1}{3})\mathbf{c}^*$ or $(l-\frac{1}{3})\mathbf{c}^*$, and destructive interference elsewhere (figs. 5 (i) and 5 (ii)). Even in electron diffraction, the $\{\mathbf{S}_M(10{\cdot}1)\}$ reflexions for the $1T_1$ and $1T_2$ phases appear only when the incident beam is a few degrees away from normal incidence to the layers (figs. 2 (i) and (ii) inset).

The interpretation of coherent scattering into the reflexions $\{\mathbf{S}_M\}$ when $l \neq 0$ for $1T_1$ and $1T_2$ requires the concept of a 'reduced deformation cell' which can only be defined statistically; its dimensions within the layer are the periods of the incommensurate distortions of the matrix lattice. As atomic positions within an infinite distorted lattice are translated into a single unit cell *of the distortion*, no two atomic positions exactly superimpose, and the situation, so far as Bragg scattering from the deformation wave is concerned, is equivalent to scattering from a continuum. In order to account for the experimental observations, these statistically defined deformation waves must be regarded as stacking rhombohedrally, even though the conventional α, β, γ positions in the distortion cell cannot be uniquely identified within the matrix structure. In $1T_1$ and $1T_2$, where $\{\mathbf{S}_M(hk\,.\,l)\}$ are referred to the local hexagonal system of reciprocal axes, the indices of observed reflexions obey the normal rhombohedral condition, $-h+k+l=3n$.

The extra reflexions on the reciprocal lattice rods parallel to $\mathbf{c}^*$ in $1T_3$ (fig. 5 (iii)) are no longer at the rhombohedral positions $(l+\frac{1}{3})\mathbf{c}^*$, indicating

that the transition to this phase from $1T_2$ has been accompanied by a change from $\alpha\beta\gamma\alpha\beta\gamma$ in the stacking sequence of distortions. If the distortions were stacked $\alpha\alpha\alpha\alpha$ in $1T_3$ then fig. 5 (iii) would show superlattice reflexions at $l\mathbf{c}^*$, and if stacked $\alpha\beta\alpha\beta$ there would be superlattice reflexions at $l\mathbf{c}^*$ and $(l+\frac{1}{2})\mathbf{c}^*$. The data are in fact consistent with the assumption that the origin of distortions in adjacent TaS_2 layers is shifted by **a**. This gives a triclinic superlattice cell whose *c*-axis is the stacking vector of the distortions, i.e. $\mathbf{c}+\mathbf{a}$. This cell may be compared with the triclinic cell for the low-temperature 1T $TaSe_2$ phase reported by Di Salvo, Maines, Waszczak and Schwall (1974). Figure 5 (iii) also shows that the crystal was twinned.

3.4. *Identification of distortion wave mode*

For a given phonon wave vector, $\mathbf{Q}$, within the TaS_2 layer there are three acoustic phonon modes (' phonon mode ' is taken to cover the case where $\omega = 0$):

(1) Longitudinal, *LA*, where $\mathbf{U}_{Q_i}$ is parallel to $\mathbf{Q}_i$ and perpendicular to $\mathbf{c}^*$.

(2) Transverse, $TA_{\parallel}$, where $\mathbf{U}_{Q_i}$ is perpendicular to $\mathbf{Q}_i$ and to $\mathbf{c}^*$.

(3) Transverse, $TA_{\perp}$, where $\mathbf{U}_{Q_i}$ is perpendicular to $\mathbf{Q}_i$ and parallel to $\mathbf{c}^*$.

It has already been shown (§ 3.1.) that to a first approximation the scattered intensity at $\mathbf{K}=\mathbf{M}+\mathbf{Q}_i$ due to a distortion of the lattice is proportional to $|(\mathbf{M}+\mathbf{Q}_i)\,.\,\mathbf{U}_{Q_i}|^2$. The increase in intensity of the $\{\mathbf{S}_M\}$ reflexions surrounding

Fig. 6

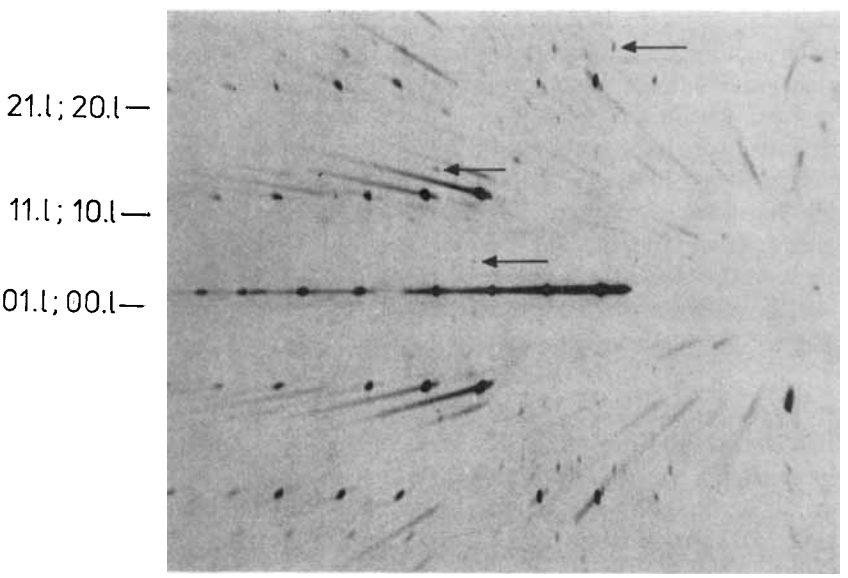

Oscillation X-ray photograph of $1T_2$ TaS_2 with incident beam perpendicular to $\mathbf{c}^*$ and recorded with a cylindrical camera. There is an increase in intensity of $\{\mathbf{S}_M\}$ reflexions (indicated by arrows) relative to the adjacent matrix reflexions, with increase in the component of scattering vector normal to $\mathbf{c}^*$.

the $M(h0 \,.\, l)$ reciprocal lattice row, with h (fig. 6) is consistent with this and confirms the original supposition of a periodic distorted structure. The experimental intensity variation of the $\{\mathbf{S}_M\}$ also makes it possible to determine the direction of $\mathbf{U}_{Q_i}$. There is very little increase in intensity of the $\{\mathbf{S}_M\}$ with index l of $M(hk \,.\, l)$ reflexions (fig. 5), from which it must be concluded that $\mathbf{U}_{Q_i} \,.\, \mathbf{c}^* \sim 0$. Therefore the displacements are *predominantly* within the TaS_2 layers so far as diffraction is concerned, and the excited modes must be LA or $TA_{\parallel}$. For a given $\mathbf{M}$, the $\{\mathbf{S}_M\}$ are most intense when $\mathbf{Q}_i$ is parallel to $\mathbf{M}$, and weakest when $\mathbf{Q}_i$ is perpendicular to $\mathbf{M}$ (figs. 3 (i), and (ii)). Thus $\mathbf{U}_{Q_i}$ must have a large component in the direction of $\mathbf{Q}_i$, and the mode is *predominantly* LA within the layer, thereby justifying the assumption of § 3.1. Furthermore, since $\mathbf{M} \,.\, \mathbf{U}_{Q_i} = 0$ for the $M(00 \,.\, l)$ reflexions, the fact that the associated $\{\mathbf{S}_M\}$ have finite intensity also argues that $\mathbf{Q}_i \,.\, \mathbf{U}_{Q_i} \neq 0$, and that LA modes constitute the major component of the layer distortion scattering incident radiation.

3.5. *Amplitude of distortion wave*

In the absence of quantitative data it is not possible to determine the amplitude of the distortion wave precisely. It is however possible to estimate its order of magnitude, from the *relative* intensities of $\{\mathbf{S}_M(10{\cdot}1)\}$ and $\{\mathbf{S}_M(11{\cdot}0)\}$ reflexions in $1T_1$ and $1T_2$ (figs. 3(i) and (ii)), since these are proportional to $U_Q{}^2$ and $U_Q{}^4$, respectively. The amplitude of the LA distortion wave in $1T_1$ is estimated to be about 0·03 Å at 400 K, and it increases continuously as the temperature is lowered in this phase. At the transition to $1T_2$ there is a discontinuous increase in U_Q to a value of about 0·1 Å. It is of interest to note that this transition temperature is lowered under hydrostatic pressure (Grant, Griffiths, Pitt and Yoffe 1974) since the ' stiffening ' of the lattice under pressure would clearly tend to inhibit this discontinuous increase in U_Q. The same approach cannot be adopted to estimate U_Q in $1T_3$ TaS_2 since the reduced deformation cell is now commensurate with the lattice. The atomic positions are defined within the $\sqrt{13}\,a \times \sqrt{13}\,a$ supercell and $\mathbf{S}_M$ loses its special significance by becoming the vector to a conventional reciprocal lattice point.

As mentioned in § 3.1., the atomic scattering factor of tantalum is much greater than that of sulphur. The values of U_Q estimated above must therefore reflect chiefly the displacements of the heavier atoms, and for the purposes of this investigation will be taken to apply only to the tantalum. Information on the sulphur positions would require more careful study, as would the detection of TA modes of relatively small amplitude.

3.6. *Diffuse scattering*

This is characteristic of the $1T_1$ phase (figs. 3 (i) and 7) and the following interpretation is consistent with the previous discussion (Williams *et al.* 1974). It can be assumed that radiation is scattered by phonons of wave vector $\mathbf{q} = 2\pi\mathbf{Q}$ and vector amplitude $\mathbf{U}_q = \mathbf{U}_Q$, and that the intensity of diffuse scattering is proportional to $|\mathbf{K} \,.\, \mathbf{U}_{Q_i}|^2$, where $\mathbf{K} = \mathbf{M} + \mathbf{Q}$. The maxima in the diffuse streaks occur where $\mathbf{K}$ is approximately perpendicular to $\mathbf{Q}$, which is consistent with the phonons being in $TA_{\parallel}$ modes (when the first Brillouin zone is taken as the frame of reference), rather than LA modes as in the case of the discrete $\{\mathbf{S}_M\}$ reflexions. Figure 7 shows that there is good

agreement between the scattering deduced for $TA_{||}$ modes from the Fermi surface proposed (fig. 8) and that observed experimentally.

Stationary and oscillation X-ray diffraction photographs did not show any intensity modulation of the diffuse scattering in the **c*** direction, so that there is no phase correlation between the $TA_{||}$ phonons in different layers. This is as expected if the diffuse streaking arises because of a dynamic rather than a static distortion. The amplitude $\mathbf{U}_Q$ of the LA modes (measured by the intensity of the $\{\mathbf{S}_M\}$) decreases as the temperature is raised from 350 K to about 450 K, whereas the amplitude of the $TA_{||}$ modes (given by the intensity of the diffuse streaking) increases to a maximum at about 380 K, before decreasing again as the temperature is further raised towards that at which the metastable $1T_1$ phase transforms to the stable 2H polytype.

Fig. 7

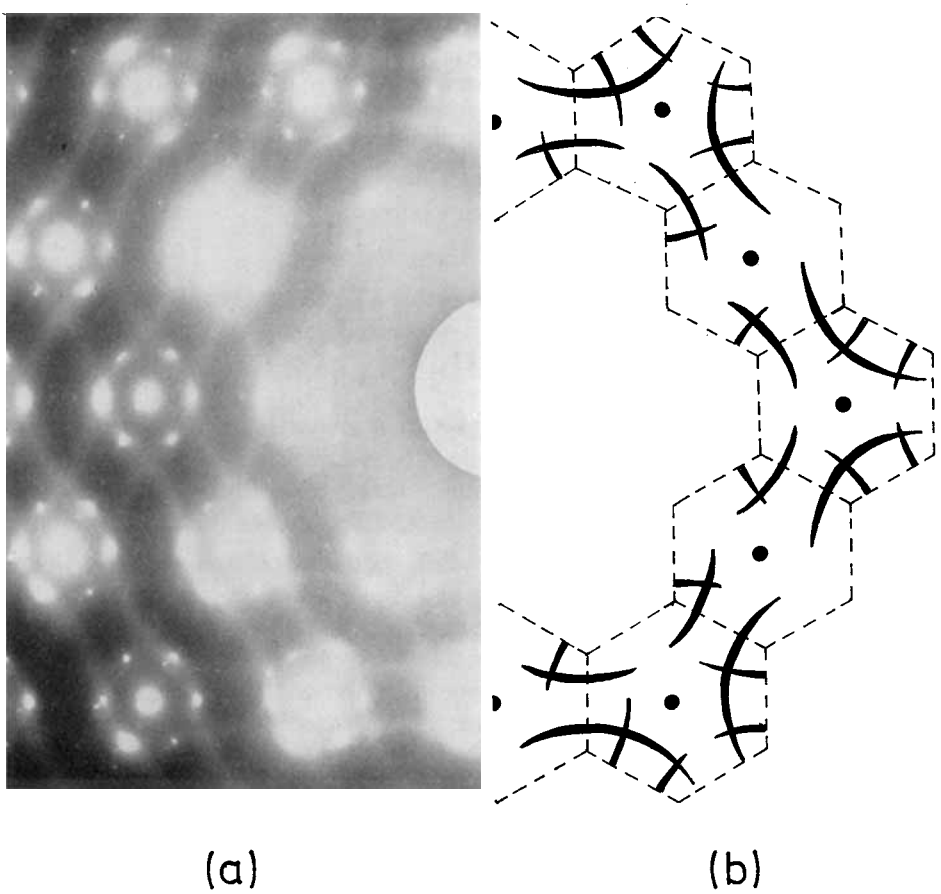

(*a*) Selected area diffraction pattern for $1T_1$ TaS_2 at 420 K, showing diffuse streaking which images the Fermi surface. All six $\mathbf{S}_M(10{\cdot}1)$ reflexions are visible because of crystal buckling. (*b*) Plot of phonon wave vectors which satisfy $\mathbf{q} \simeq 2\mathbf{k}_F$ for 1T TaS_2 Fermi surface (see fig. 8), and are in $TA_{||}$ modes with $|\mathbf{k} \cdot \mathbf{U}_q|^2$ large.

Fig. 8

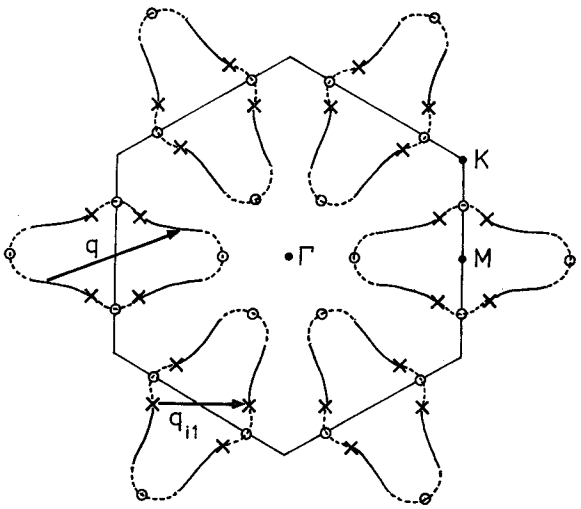

ΓKM section of 1T TaS_2 Brillouin zone, the six segments of Fermi surface enclosing filled electron states. The parts of the surface imaged in diffraction by $TA_{\parallel}$ phonons (such as $\mathbf{q}$) are drawn as solid lines; $\mathbf{q}_{i1}$ is the wave vector of a condensed LA mode in $1T_1$. ○—k_F inferred from band structure calculations (Mattheiss 1973); ×—k_F from diffraction data (Williams, Parry, Scruby 1974).

§ 4. Discussion

4.1. *Structural*

The CdI_2-type (C6) structure of the stable 1T phase (above 1050 K) undergoes characteristic deformations when quenched; three separate metastable phases have been identified: $1T_1$, $1T_2$, $1T_3$.

$1T_1$: (350 to ~450 K). The 1T structure is modulated by incommensurate periodic distortions (amplitude ~0·03 Å) arising from softened LA modes. These distortions stack rhombohedrally. There are also partially softened phonons in selected $TA_{||}$ modes.

$1T_2$: (190 to 350 K). The softened $TA_{||}$ modes associated with the diffuse streaking have disappeared and the distortion wave vector has changed discontinously in orientation and amplitude (~0·1 Å). The distortion wave vector is now temperature-dependent, and its magnitude and orientation vary more rapidly as the temperature of the transition to $1T_3$ approaches. The periodic distortions maintain rhombohedral stacking.

$1T_3$: (below 190 K). The ' distortions ' in this phase are commensurate with the matrix lattice and define a superlattice with a $\sqrt{13}\,a \times \sqrt{13}\,a$ unit cell. The layer distortions no longer stack rhombohedrally, and this superlattice is triclinic.

The $1T_1 \rightarrow 1T_2$ and $1T_2 \rightarrow 1T_3$ transformations occur in the same regions of temperature as the transitions reported by Thompson *et al.* (1971) from electrical

measurements. To illustrate a modulated matrix structure, single layers of Ta atoms are shown in fig. 9 as they might appear in each of the three metastable phases if $U_Q = 0{\cdot}1\ a$. The broken lines define the distortion ' cell ' in each case, and in the absence of data on the relative phases of the three distortion waves, the nodes in each wave have been made to coincide at a point. In the incommensurate cases the choice of origin is arbitrary, while in $1T_3$ the origin is chosen to be at a metal atom site.

Fig. 9

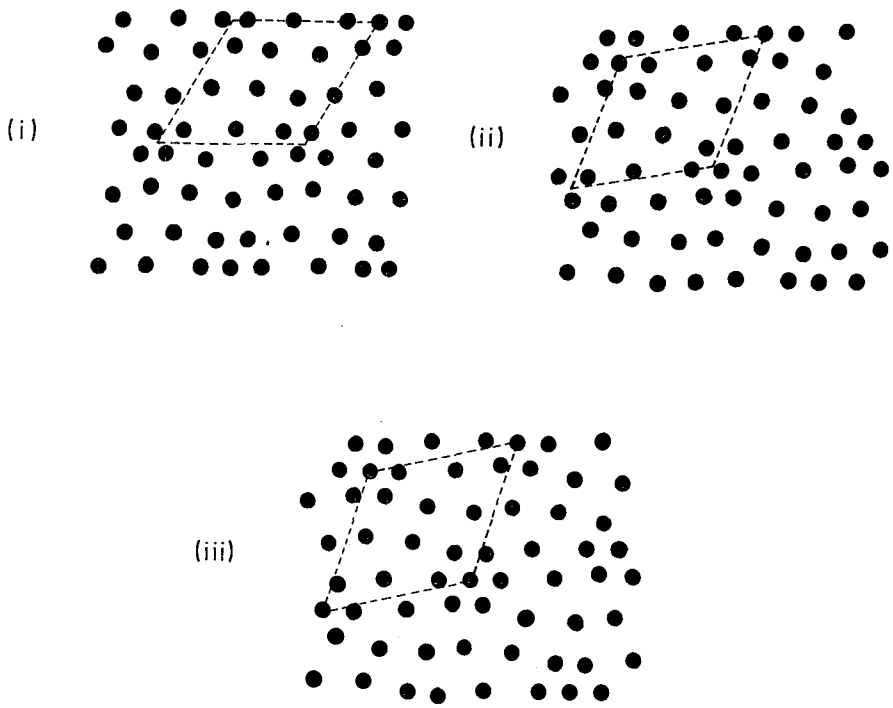

Model for single layers of Ta atoms in each distorted TaS_2 phase ($U_Q \simeq 0{\cdot}1\ a$). Origin of distortion ' cell ' (broken lines) arbitrary in the incommensurate $1T_1$ (i), and $1T_2$ (ii), at metal atom site in $1T_3$ (iii).

The origins of the distortions in terms of an electronic charge density wave will be discussed in the next section: for the present, it will be assumed that the charge density wave and the lattice distortion are in phase so that charge is localized in regions of increased ion core density, thereby fulfilling screening requirements (Overhauser 1968, Chan and Heine 1973). In the case of a commensurate periodic distortion ($1T_3$) it is always possible for the charge maxima to coincide with metal atoms, whereas for an incommensurate distortion wave, charge tends to be localized both close to and away from metal sites. This alternation of localized electronic charge between different sites could be expected to raise the electrostatic energy. The alternation occurs more frequently in $1T_1$ than in $1T_2$ and, as might be anticipated from electrostatic considerations, the amplitude of the distortion wave increases in $1T_2$. The atomic displacements would be expected to be greatest in $1T_3$, since in this

commensurate phase all the charge maxima are on metal sites. In all three phases, variations in bond lengths and bond angles change the symmetry of the metal atom environments.

As noted in § 3.5 it is difficult to infer anything from the present experimental data about the positions of the sulphur atoms in the distorted lattice. However, by comparison with the distorted tellurides of groups Va and VIa (Brown 1966), the chalcogens might be expected to be drawn in towards the metal layer when the Ta–Ta separation increases, and pushed away as the Ta atoms come closer together. Such displacements of sulphur atoms in the c-axis direction are equivalent to coupling with a TA_1 mode, but there is no diffraction evidence to suggest that such a mode has an easily detectable amplitude. However, such distortions would vary the ' thickness ' of the layers and successive layers would need to be translated in order to minimize the volume of the crystal. This suggests an explanation of the rhombohedral packing of distortions in $1T_1$ and $1T_2$.

Although periodic variations of layer ' thickness ' might be expected within the superlattice cell of $1T_3$, rhombohedral stacking of such irregularities would prevent the charge density wave maxima from being localized at ideal metal sites. For example, if an α site of the $\sqrt{13}\,a \times \sqrt{13}\,a$ supercell is located at a Ta atom, then the β and γ sites correspond to interstitial sites adjacent to sulphur atoms. The maxima can only be on Ta sites in every layer if there is a stacking change in the charge density waves and so in the lattice distortions which stabilize them. Although there are 13 Ta atoms in the layer superlattice cell, each in principle able to be the origin of the charge density wave, the hexagonal symmetry of the layer reduces the number of different sites to three, the corresponding stacking vectors being $\mathbf{c}$ (giving $\alpha\alpha\alpha\alpha$ stacking), $\mathbf{c}+\mathbf{a}$, $\mathbf{c}+2\mathbf{a}$. The latter two both have triclinic superlattice cells and form 13-layer stacks. Diffraction evidence favours the cell with stacking vector $\mathbf{c}+\mathbf{a}$ (see § 3.3.). Considerable stacking disorder and twinning (with stacking vector $\mathbf{c}-\mathbf{a}$) would be expected, and experimental evidence supports this. As a consequence of the change from minimum volume $\alpha\beta\gamma\alpha\beta\gamma$ stacking a slight increase in the crystal c-axis dimension might be expected as a result of the variations in layer thickness, and indeed a discontinuous increase of 0·02 Å in c is detected as the temperature of the crystal is lowered through the $1T_2 \rightarrow 1T_3$ transition (Thompson *et al.* 1971).

4.2. *Electronic*

As previously reported (Williams *et al.* 1974) the distortions discussed above may be interpreted as arising from a Kohn anomaly possibly enhanced by electron–hole interaction. The divergence in the static electronic susceptibility $\chi(\mathbf{q})$ at $\mathbf{q}=2\mathbf{k}_F$ may lead to the formation of a charge density wave which has been shown to be unstable except in the presence of a periodic lattice distortion (Chan and Heine 1973). Thus, in fig. 8, the measured distortion wave vector, $\mathbf{q}_{i1}$, just spans one piece of the proposed Fermi surface. If the diffuse scattering of X-rays and electrons in the $1T_1$ phase is then to be regarded as an image of this surface in the phonon spectrum, the conditions required for adequate contrast deserve further consideration. Enhanced Kohn scattering requires large radii of curvature of the Fermi surface (Afanasev

and Kagan 1963, Fehlner and Loly 1974), and this condition is met in the k_z direction of the surface proposed earlier on the basis of the calculations of Mattheiss (1973). Even so, the image does not reveal the curved ends of the electron segments lying along ΓM in the ΓKM section (fig. 8) and it must be concluded that the radius of curvature within the plane for this region is too small to strengthen the Kohn anomaly sufficiently for the associated phonons to be visible in diffraction. It is noteworthy that all other parts of the observed image have large radii of curvature, and in fact the image is consistent with a change in sign of the latter, as is seen in fig. 7. The large radii ($\rightarrow\infty$) at such points of inflection would permit perfect nesting and maximum softening of the phonon modes with wave vector $\mathbf{q} = 2\mathbf{k}_F$, close to the observed $\mathbf{q}_{i1}$.

Only the LA modes appear to be completely softened in the $1T_1$ phase, and indeed even this assertion requires confirmation by neutron scattering experiments. In the case of the $TA_{||}$ modes, the electron–phonon coupling must be weaker since these modes are only partially softened and no correlation between distortions in successive layers is detectable. In the $1T_2$ phase, which occurs on merely cooling $1T_1$, the long-range order between the static LA distortions in successive layers remains, but the sudden disappearance of the diffuse X-ray and electron scattering at the transition indicates that the $TA_{||}$ modes are incorporated into the static distortions.

It is interesting to compare these conclusions with the results obtained from studies of the one-dimensional conductor $K_2Pt(CN)_4Br_{0\cdot3} \cdot 3H_2O$. In this case a linear superlattice distortion is observed at room temperature by X-ray diffuse scattering (Comes, Lambert, Launois and Zeller 1973); and neutron scattering experiments (Renker, Pintschovius, Gläser, Rietschel, Comes, Liebert and Drexel 1974) have sugested that this distortion involves both a dynamic Kohn anomaly and a static Peierls distortion (Peierls 1955). When cooled to below 120 K, the deformations in adjacent chains begin to order in antiphase alignment but unlike 1T TaS_2 long-range ordering is not achieved even at 6 K. Even in the most ordered state, orientational correlation is lost after about 30 Å, i.e. after about three chains.

The variation in electrical resistivity of $K_2Pt(CN)_4Br_{0\cdot3} \cdot 3H_2O$ which accompanies these structural changes ($10^{-2}\,\Omega$ cm at room temperature to $10^{12}\,\Omega$ cm at 20 K, according to Kuse and Zeller 1971) agrees well with a transition from a metallic to a Peierls insulating state. The situation in 1T TaS_2 is far less clear: the $1T_1$ phase exhibits metallic conductivity (Thompson *et al.* 1971) while, with a resistivity of $\sim 10^{-2}\,\Omega$ cm, $1T_3$ seems likely to be semiconducting (fig. 1). The behaviour of the intermediate phase $1T_2$ is somewhat harder to characterize. The resistivity of $1T_2$ ($\sim 10^{-3}\,\Omega$ cm) is closer to that of the metallic phase than to $1T_3$, and although Thompson *et al.* (1971) characterized both $1T_2$ and $1T_3$ as narrow-gap semiconductors, in a later paper Thompson, Pisharody and Koehler (1972) pointed out that in both phases the activation energy for conduction is less than kT, and that in neither phase does the resistivity variation fit an Arrhenius plot over a significant temperature interval.

In the presence of the charge density wave and periodic lattic distortion, however, the conduction mechanism in all three phases is likely to be more complex than in either a simple metal or a semiconductor, since by analogy with one-dimensional systems (Fröhlich 1954, Peierls 1955, Lee, Rice and

Anderson 1974) a gap in the electronic energy spectrum would be expected around at least part of the Fermi surface. The discontinuous increase in U_q between $1T_1$ and $1T_2$ is consistent with a first-order change in the magnitude and extent of this gap and hence with the increase in resistivity; the behaviour of the latter within the $1T_2$ phase may then reflect the temperature dependence of the gap. A similar argument can be applied to the transition between $1T_2$ and $1T_3$, and it is possible in the latter case that the gap extends around the whole of the Fermi surface, making the material semiconducting. Certainly in the related case of 1T $TaSe_2$ Wilson, di Salvo and Mahajan (1974 b) have estimated that the reconstruction on formation of the perfect $\sqrt{13}\,a \times \sqrt{13}\,a$ superlattice destroys at least 90% of the Fermi surface.

It is of interest to examine the comparison between 1T TaS_2 and 1T $TaSe_2$ in greater detail. The most important difference is that the intermediate phase ($1T_2$) does not occur in the selenide; its absence would appear to be due to differences in Fermi surface geometry between the two materials. Thus the $\mathbf{q}_1$ which spans the surface in $1T_1$ TaS_2 immediately above the transition ($0{\cdot}283\,\mathbf{a}^*$) is larger than the equivalent $\mathbf{q}_1$ in $1T_1$ $TaSe_2$ ($\mathbf{a}^*/3{\cdot}6 = 0{\cdot}278\mathbf{a}^*$, according to Wilson *et al.* 1974). The reciprocal lattice vector corresponding to the $\sqrt{13}\,a$ coincidence cell then lies very close to the Fermi surface in the selenide. Thus at the transition, the $\mathbf{q} = 2\mathbf{k}_f$ wave vector can switch to the coincidence reciprocal cell vector and so impose a commensurate Peierls-like distortion on the structure that is observed experimentally as a $\sqrt{13}\,a \times \sqrt{13}\,a$ superlattice. On the other hand, at the $1T_1$–$1T_2$ transition in the sulphide, the Fermi surface in the ΓKM section has a larger cross section, so that the coincidence cell vector ($0{\cdot}277a^*$) cannot span the surface, but lies within it; consequently a neighbouring but still incommensurate spanning vector $\mathbf{q}_2$ must be selected (fig. 10). Provided the wave vector rotates away from the KM direction, then throughout the $1T_2$ phase, it spans the Fermi surface where it is almost flat, maintaining the strength of the Kohn anomaly.

On reducing the temperature further, this vector swings round (fig. 10) and changes in magnitude until, at about 190 K, it can become the coincidence vector of the $1T_3$ phase. This change in $\mathbf{q}_2$ with temperature must mean that the Fermi surface is shrinking back towards the M point on the zone boundary, which implies either that there is a reduction in the number of carriers as the temperature is lowered, or that the surface is changing in shape. Since the wave vector in 1T $TaSe_2$ is able to switch directly to the $\sqrt{13}\,a$ coincidence cell at the one transition, then the Fermi surface in this material must be similar to that in the sulphide at the $1T_2$–$1T_3$ transition temperature, i.e. BB' in fig. 10. Recent photoemission studies (Shepherd and Williams 1974) are consistent with a small overlap between the d like condution electrons and the p-like valence band in 1T TaS_2, so that the density of occupied states at the Fermi level could exhibit the required temperature variation as a result of changes in d–p overlap.

It should be noted that a reduction in carriers would again contribute to the anomalous resistivity behaviour within the $1T_2$ phase, independently of any consideration of a temperature-dependent energy gap. Furthermore, such a correlation between the magnitude of the distortion wave vector and the carrier density has been demonstrated by Wilson *et al.* (1974 a) for the mixed system $Ta_xTi_{1-x}S_2$; the increase in spanning vector in 1T TaS_2 on intercalation with

Fig. 10

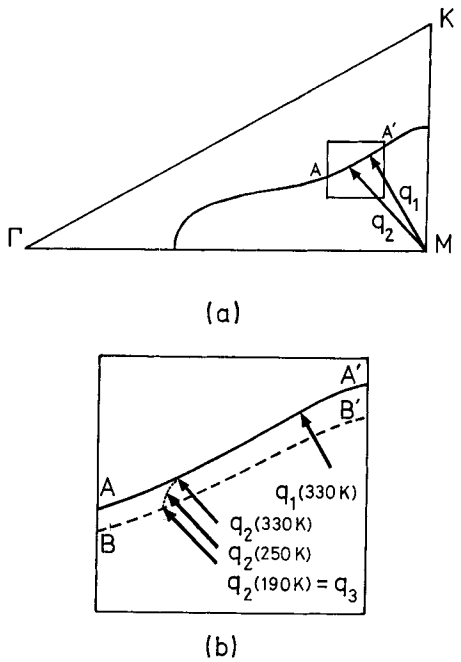

(*a*) Part of one segment of 1T TaS_2 Fermi surface at 330 K. (*b*) More detailed diagram of the switch from $\mathbf{q}_1$ to $\mathbf{q}_2$ at 330 K, and the proposed shrinking of the surface from AA' to BB' on lowering the temperature to 190 K, with $\mathbf{q}_2$ changing magnitude and direction until it locks onto the commensurate $\mathbf{q}_3$ (defining $\sqrt{13}\,a$ coincidence).

Na (which donates an electron, thereby increasing the size of the Fermi surface) provides similar confirmation (Mr. W. B. Clarke 1974, private communication). However, it is not easy to see how the required change in carrier density with temperature (to produce a 5% change in q_2) can be accomplished within $1T_2$; certainly, the possiblility of a change in shape of the Fermi surface, for example following touching of neighbouring segments as the temperature is varied (Hughes and Liang 1974), cannot be excluded as an explanation of the change in wave vector.

In conclusion, it may be noted that charge density wave behaviour is observed in other group IV_a and V_a layer dichalcogenides such as $NbSe_2$ (Shepherd *et al.* 1974, Wilson di Salvo and Mahajan 1974 b). Direct confirmation with neutron scattering experiments of Kohn anomalies and phonon mode softening in these materials is awaited with interest.

Acknowledgments

The authors wish to thank Dr. F. Levy (École Polytechnique Fédérale de Lausanne) and Dr. F. Gamble (Exxon Research and Engineering Company) for the supply of single crystals, and Mrs. B. A. Robinson for assistance with the electron microscopy. They are also grateful to Dr. A. D. Yoffe, Dr. A. J. Grant and Professor R. Comes for stimulating discussions, and to the Science Research Council for financial support.

References

Afanasev, A. M., and Kagan, Y., 1963, *Soviet Phys. JETP*, **16,** 1030.

Bacon, G. E., 1962, *Neutron Diffraction* (Oxford: Clarendon Press).

Brown, B. E., 1966, *Acta crystallogr.*, **20,** 264.

Chan, S.-K., and Heine, V., 1973, *J. Phys.* F, **3,** 795.

Comes, R., Lambert, M., Launois, H., and Zeller, H. R., 1973, *Phys. Rev.* B, **8,** 2, 571.

Di Salvo, F. J., Maines, R. G., Waszczak, J. V., and Schwall, R. E., 1974, *Solid St. Commun.*, **14,** 497.

Fehlner, W. R., and Loly, P. D., 1974, *Solid St. Commun.*, **14,** 653.

Fröhlich, H., 1954, *Proc. R. Soc.* A, **223,** 296.

Grant, A. J., Griffiths, T. M., Pitt, G. D., and Yoffe, A. D., 1974, *J. Phys.* C, **7,** L249.

Hughes, H., and Liang, W. Y., 1974, *J. Phys.* C, **7,** L162.

James, R. W., 1948, *The Optical Principles of the Diffraction of X-rays* (London: Bell).

Jellinek, F., 1962, *J. Less-common Metals*, **4,** 9.

Kohn, W., 1959, *Phys. Rev. Lett.*, **2,** 393.

Kuse, D., and Zeller, H. R., 1971, *Phys. Rev. Lett.*, **27,** 1060.

Lee, P. A., Rice, T. M., and Anderson, P. W., 1974, *Solid St. Commun.*, **14,** 703.

Mattheiss, L. F., 1973, *Phys. Rev.* B, **8,** 3719.

Overhauser, A. W., 1962, *Phys. Rev.*, **128,** 1437; 1968, *Ibid.*, **167,** 3, 692; 1971, *Ibid.* B, **3,** 10, 3173.

Peierls, R. E., 1955, *Quantum Theory of Solids* (Oxford: Clarendon Press).

Renker, B., Pintschovius, L., Gläser, W., Rietschel, H., Comes, R., Liebert, L., and Drexel, W., 1974, *Phys. Rev. Lett.*, **32,** 15, 836.

Shepherd, F. R., and Williams, P. M., 1974, *J. Phys.* C (to be published).

Shepherd, F. R., Williams, P. M., Young, D. A., and Scruby, C. B., 1974, *Proceedings of XIIth International Conference on the Physics of Semiconductors*, Stuttgart, edited by M. H. Pilkhun (Stuttgart: Teubner).

Thompson, A. H., Gamble, F. R., and Revelli, J. F., 1971, *Solid St. Commun.*, **9,** 981.

Thompson, A. H., Pisharody, K. R., and Koehler, R. F., 1972, *Phys. Rev. Lett.*, **29,** 3, 163.

Williams, P. M., Parry, G. S., and Scruby, C. B., 1974, *Phil. Mag.*, **29,** 695.

Wilson, J. A., Di Salvo, F. J., and Mahajan, S., 1974 a, *Phys. Rev. Lett.*, **32,** 16, 882; 1974 b, *Phys. Rev.* (to be published).

Wilson, J. A., and Yoffe, A. D., 1969, *Adv. Phys.*, **18,** 193.